Available online at www.sciencedirect.com
SCIENCE DIRECT®
Journal of Sound and Vibration 286 (2005) 849–867
JOURNAL OF SOUND AND VIBRATION
www.elsevier.com/locate/jsvi

Stability of elastic columns with periodic retarded follower forces

Haitao Ma[1], Eric A. Butcher*

Department of Mechanical Engineering, University of Alaska Fairbanks, Fairbanks, AK 99775, USA

Received 16 June 2003; received in revised form 4 October 2004; accepted 21 October 2004
Available online 18 January 2005

Abstract

The objective of this work is to present a stability analysis for elastic columns under the influence of periodically varying follower forces whose orientation is retarded, i.e., depends on the position of the system at a previous time. One- and two-degree-of-freedom (dof) discretized systems under the simultaneous influence of both parametric excitation and time-delay, whose effects on such systems have previously been only considered separately, are studied. By employing an orthogonal polynomial approximation, the *infinite-dimensional Floquet transition matrix* associated with the time-periodic differential-delay system is approximated. The stability criteria that all the eigenvalues (Floquet multipliers) of this matrix must lie within the unit circle is then applied. The stability charts for different combinations of the remaining system parameters are shown, and the previously reported results for the special cases where either the parametric excitation or the time-delay vanishes are verified. Two cases, when the parametric forcing period is equal to or twice the delay period are taken into consideration in this work. For special cases of the single dof system, the numerical stability plots are verified by considering the analytical expressions for the corresponding stability boundaries for an analogous delayed Mathieu equation.

*Corresponding author.
E-mail address: ffeab@uaf.edu (E.A. Butcher).
[1]Present address. Control Contractors Inc., Fairbanks, AK 99708, USA.

0022-460X/$ - see front matter © 2004 Elsevier Ltd. All rights reserved.
doi:10.1016/j.jsv.2004.10.052

1. Introduction

The stability analysis of elastic systems subjected to nonconservative follower forces is of great interest in various engineering fields. After Beck's well-known paper in 1952 which analyzed what later became known as Beck's column [1], several important monographs and papers revisited this important topic [2–4]. Several properties of such systems have been identified, including the possibility of failure due to flutter instability [4] and the potentially destabilizing effect of damping [5], which are not present in conservative elastic systems in which only divergence instability is present and damping is a stabilizing effect. The fact that stability analyses for nonconservative systems must necessarily take the dynamics of such systems into account is an additional complication which conservative systems that can be analyzed statically do not exhibit. Using the modern language of dynamical systems, a nonlinear nonconservative system may experience a *Hopf bifurcation* (dynamic instability) in addition to a *saddle–node* bifurcation (static instability) [6]. Furthermore, not all nonconservative systems may exhibit flutter or Hopf bifurcation. Husseyin [7] classifies such systems as either pseudo-conservative or circulatory, depending on whether the asymmetric stiffness matrix can be symmetrized through an appropriate transformation. If it cannot, then it is circulatory and may experience flutter [7].

More recently, the analysis of elastic systems subjected to nonconservative follower forces has been extended in two directions. First, the introduction of a time-delay in the angle of the follower force such that its orientation depends on the state of the system at a previous (delayed) time instead of the present time has been considered in various studies, e.g. Refs. [8–10]. The mathematical models for such systems are delay-differential equations (DDEs), and the stability analysis is complicated by the fact that such equations have transcendental characteristic equations with an infinite number of roots (eigenvalues). Nevertheless, several stability theorems have been formulated for such systems, including the Pontryagin, D-subdivision and tau-decomposition methods [8,9]. Both single- and 2 dof undamped inverted pendulums with delayed follower forces were considered in Ref. [9] whereas in Refs. [8,10] the effect of damping on the 2 dof system was analyzed. It was found in these studies that the presence of a very small time delay can be enough to cause instability if the damping is small or nonexistent. The instability routes are due to both the saddle–node and Hopf bifurcations as in the systems with nondelayed follower forces.

The second direction that has been pursued has been to consider the effect of follower forces with periodically varying magnitudes. This introduces time-periodic coefficients (parametric excitation) to the ordinary differential equations and thus requires the use of Floquet theory [11] for stability analysis. By computing the fundamental solution matrix at the end of the principal period of excitation (either by direct numerical integration or symbolically in terms of parameters as in Refs. [12,13]), the Floquet transition matrix is obtained whose eigenvalues are the Floquet multipliers which must lie within the unit circle in the complex plane for asymptotic stability. Butcher and Sinha [12] computed the stability chart for the 2 dof inverted pendulum problem both numerically and symbolically and showed the existence of parametric resonance instability regions as well as a third type of instability due to period doubling. This "flip bifurcation" is associated with Floquet multipliers leaving the unit circle at -1 in the complex plane and does not occur for time-invariant systems [11]. It was shown in Ref.

[12] that the effect of damping is to "lift" the instability regions due to parametric excitation, thus enlarging the stability region.

The simultaneous effect of both time-delay and parametric excitation on elastic systems with nonconservative follower forces has not been previously considered as the associated time-periodic DDEs incorporate both time-delay and periodic coefficients. An infinite-dimensional extension of Floquet theory, however, does exist for such systems in which the eigenvalues of the monodromy operator, or "infinite-dimensional Floquet transition matrix", determine the stability. Recently, a few numerical techniques have been developed to construct an approximate finite-dimensional version [14–16]. It was recently shown in Ref. [14] that, by using shifted Chebyshev polynomials and the associated operational matrices, the periodic DDE system can be reduced to a set of difference equations from which a finite-dimensional approximation of the monodromy operator is found. For the special case in which the delay and parametric periods are equal, this matrix defines a linear map which transforms the Chebyshev coefficients of the state in the previous delay interval to the Chebyshev coefficients of the state in the present delay interval. Therefore, the stability criteria is that all the eigenvalues of this matrix should fall inside the unit circle in the complex plane. An extension to the case where the parametric and delay periods are rationally related is also available.

In this paper, this technique is used to analyze the stability of elastic columns with nonconservative follower forces which contain both parametric excitation and time lag. The stability charts for single and double inverted pendulums subjected to retarded periodic follower forces are produced by applying the stability criteria described above. The charts are shown for a variety of different parameter values for various amounts of damping and angular positions of the follower force. The previously reported results for the cases where either the parametric excitation or the time-delay vanishes are verified. It is shown that as the magnitude of periodic excitation is increased, the stable region is decreased as a result of the effect of parametric resonances. The numerical stability results are verified by the analogous analytical stability boundaries of a delayed Mathieu equation. It is shown that this technique offers an efficient and accurate way to study the stability properties of this class of systems.

2. Equations of motion

2.1. Elastic column

Fig. 1 shows an elastic column with elastic modulus EI, density ρ, and length l, which is clamped at the base. It is subjected to a nonconservative follower load at the opposited end whose magnitude consists of both constant and time periodic components and which acts at an angle proportional (by a constant γ) to the slope at that end at a previous time $t-\tau$. P_1 and $P_2\cos\omega t$ are the constant and time-periodic parts of the follower force, ω is the parametric forcing frequency, and τ is a constant delay period. Neglecting shear and inertia effects and assuming small displacements and linear viscous damping, the equation of motion for the deflection $y(x,t)$

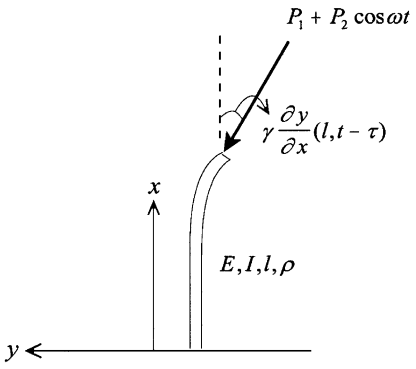

Fig. 1. An elastic column subjected to a periodic retarded follower force.

can be derived as

$$EIy''''(x,t) + (P_1 + P_2\cos\omega t)y''(x,t) + \rho\ddot{y}(x,t) + c\dot{y}(x,t) = 0, \tag{1}$$

$$y(0,t) = 0, \quad y'(0,t) = 0,$$

$$y''(l,t) = 0, \quad (P_1 + P_2\cos\omega t)(y'(l,t) - \gamma y'(l,t-\tau)) = -EIy'''(l,t).$$

Eq. (1) is a linear partial differential equation with time-periodic coefficients with a boundary condition which contains both time-periodic coefficients and time-delay. Because the stability analysis of this system is extremely difficult, we instead choose to analyze discretized versions of the problem which give rise to ODEs with time-periodic coefficients and time-delay for which an infinite-dimensional version of Floquet theory may be applied. Therefore, we will consider both single and double inverted pendulum approximations to the elastic column.

2.2. A single inverted pendulum

A single dof inverted pendulum subjected to a parametrically excited and retarded follower force is first considered. The diagram of the mechanical system is shown in Fig. 2(a) in which $q(t)$ denotes the angle coordinate (measured from vertical position), γ is the load direction parameter, k is the torsional stiffness, c is the damping constant, m is the mass at the end of the weightless beam which has the length l, P_1 and P_2 are the constant and time-periodic parts of the follower force, and ω is the parametric forcing frequency. The equation of motion for this system can be derived as

$$ml^2\ddot{q}(t) + kq(t) + c\dot{q}(t) - (P_1 + P_2\cos\omega t)l\sin(q(t) - \gamma q(t-\tau)) = 0. \tag{2}$$

The linearized equation about $q = 0$ is

$$ml^2\ddot{q}(t) + c\dot{q}(t) + (k - (P_1 + P_2\cos\omega t)l)q(t) + (P_1 + P_2\cos\omega t)l\gamma q(t-\tau) = 0. \tag{3}$$

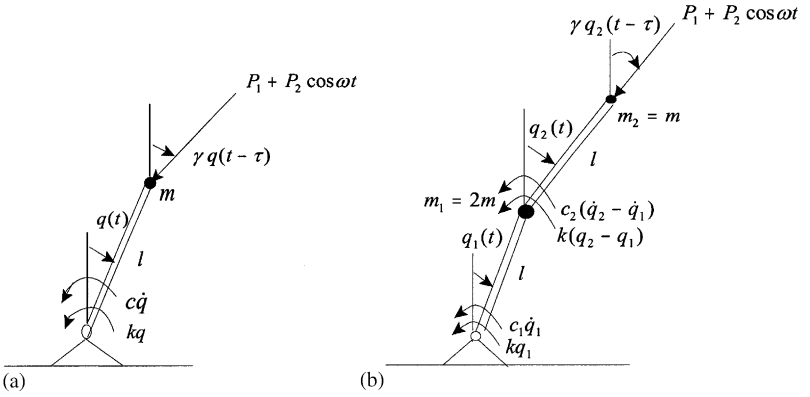

Fig. 2. (a) A simple inverted pendulum, (b) a double inverted pendulum subjected to periodic retarded follower force.

Normalizing the delay period τ to 1 by defining a new time coordinate $\hat{t}$ such that $t = \tau\hat{t}$ and denoting $x_1 = q, x_2 = \dot{q}$, we rewrite Eq. (3) into state-space form as

$$\begin{pmatrix} \dot{x}_1 \\ \dot{x}_2 \end{pmatrix} = \begin{bmatrix} 0 & 1 \\ -\hat{\tau}^2(1 - \hat{P}_1 - \hat{P}_2\cos\omega\tau\hat{t}) & -\hat{\tau}\bar{c} \end{bmatrix} \begin{pmatrix} x_1 \\ x_2 \end{pmatrix} + \begin{bmatrix} 0 & 0 \\ -\hat{\tau}^2(\hat{P}_1 + \hat{P}_2\cos\omega\tau\hat{t})\gamma & 0 \end{bmatrix} \begin{pmatrix} x_1(\hat{t}-1) \\ x_2(\hat{t}-1) \end{pmatrix}, \tag{4}$$

where $\hat{P}_1 = P_1 l/k,\ \hat{P}_2 = P_2 l/k,\ \hat{\tau} = \alpha\tau,\ \alpha = \sqrt{k/(ml^2)},\ \bar{c} = \alpha c/k$.

This is similar to the single dof problem studied in Ref. [9]. However, in this case both periodic excitation and time-delay effects are taken into consideration, whereas only time-delay was present in Ref. [9].

2.3. Double inverted pendulum

Next, we consider a two dof double inverted pendulum subjected to a periodic follower force with time delay. Fig. 2(b) shows the mechanical system. The system has two rigid weightless bars with equal lengths l with two masses $m_1 = 2m$ and $m_2 = m$ attached at their ends. $q_1(t)$ and $q_2(t)$ are the angular coordinates, c_1 and c_2 are the damping constants, k is a torsional spring constant, γ is the load direction parameter, P_1 and P_2 are the constant and time-periodic part of the follower force and ω is the parametric forcing frequency. The equations of motion can be expressed as

$$3ml^2\ddot{q}_1(t) + ml^2\cos(q_2(t) - q_1(t))\ddot{q}_2(t) - \sin(q_2(t) - q_1(t))\dot{q}_2(t)^2 + (c_1 + c_2)\dot{q}_1(t) - c_2\dot{q}_2(t) + 2kq_1(t) - kq_2(t) - (P_1 + P_2\cos\omega t)l\sin(q_1(t) - \gamma q_2(t-\tau)) = 0, \tag{5a}$$

$$ml^2\cos(q_2(t) - q_1(t))\ddot{q}_1(t) + ml^2\ddot{q}_2(t) + \sin(q_2(t) - q_1(t))\dot{q}_1(t)^2 - c_2\dot{q}_1(t) + c_2\dot{q}_2(t) - kq_1(t) + kq_2(t) - (P_1 + P_2\cos\omega t)l\sin(q_2(t) - \gamma q_2(t-\tau)) = 0. \tag{5b}$$

The linearized equations of motion about the $q_1 = q_2 = 0$ equilibrium position are

$$3ml^2\ddot{q}_1(t) + ml^2\ddot{q}_2(t) + (c_1 + c_2)\dot{q}_1(t) - c_2\dot{q}_2(t) + 2kq_1(t) - kq_2(t) - (P_1 + P_2\cos\omega t)lq_1(t) + (P_1 + P_2\cos\omega t)l\gamma q_2(t-\tau) = 0, \tag{6a}$$

$$ml^2\ddot{q}_1(t) + ml^2\ddot{q}_2(t) - c_2\dot{q}_1(t) + c_2\dot{q}_2(t) - kq_1(t) + kq_2(t) - (P_1 + P_2\cos\omega t)lq_2(t) + (P_1 + P_2\cos\omega t)l\gamma q_2(t-\tau) = 0. \tag{6b}$$

Normalizing the delay period to 1 via $t = \tau\hat{t}$ and denoting $x^{\mathrm{T}} = (x_1\ x_2\ x_3\ x_4) = (q_1\ q_2\ \dot{q}_1\ \dot{q}_2)$, Eqs. (6a) and (6b) are rewritten into state-space form (following premultiplication by the inverse of the mass matrix) as

$$\begin{pmatrix} \dot{x}_1 \\ \dot{x}_2 \\ \dot{x}_3 \\ \dot{x}_4 \end{pmatrix} = \begin{bmatrix} 0 & 0 & 1 & 0 \\ 0 & 0 & 0 & 1 \\ -\hat{\tau}^2(1.5 - 0.5\hat{P}_1 - 0.5\hat{P}_2\cos\omega\tau\hat{t}) & -\hat{\tau}^2(-1 + 0.5\hat{P}_1 + 0.5\hat{P}_2\cos\omega\tau\hat{t}) & -\hat{\tau}(0.5\bar{c}_1 + \bar{c}_2) & -\hat{\tau}(-\bar{c}_2) \\ -\hat{\tau}^2(-2.5 + 0.5\hat{P}_1 + 0.5\hat{P}_2\cos\omega\tau\hat{t}) & -\hat{\tau}^2(2 - 1.5\hat{P}_1 - 1.5\hat{P}_2\cos\omega\tau\hat{t}) & -\hat{\tau}(-0.5\bar{c}_1 - 2\bar{c}_2) & -\hat{\tau}(2\bar{c}_2) \end{bmatrix} \times \begin{pmatrix} x_1 \\ x_2 \\ x_3 \\ x_4 \end{pmatrix} + \begin{bmatrix} 0 & 0 & 0 & 0 \\ 0 & 0 & 0 & 0 \\ 0 & 0 & 0 & 0 \\ 0 & -\hat{\tau}^2(\hat{P}_1 + \hat{P}_2\cos\omega\tau\hat{t})\gamma & 0 & 0 \end{bmatrix} \begin{pmatrix} x_1(\hat{t}-1) \\ x_2(\hat{t}-1) \\ x_3(\hat{t}-1) \\ x_4(\hat{t}-1) \end{pmatrix}, \tag{7}$$

where $\hat{P}_1 = P_1 l/k, \hat{P}_2 = P_2 l/k, \hat{\tau} = \alpha\tau, \alpha = \sqrt{k/(ml)}, \bar{c}_1 = \alpha c_1/k, \bar{c}_2 = \alpha c_2/k$.

Restricted versions of this problem were studied before in Refs. [8,9,12]. However, it should be noted that in Refs. [8,9], there is no time-periodic excitation, while in Ref. [12] there is no time-delay.

3. Method of analysis

Eqs. (4) and (7) have the same form as

$$\dot{\mathbf{x}}(t) = \mathbf{A}_1(t)\mathbf{x}(t) + \mathbf{A}_2(t)\mathbf{x}(t-\tau),$$

$$\mathbf{x}(t) = \phi(t), \quad t_0 - \tau \leqslant t \leqslant t_0, \tag{8}$$

where $\mathbf{x}(t)$ is the $n \times 1$ state vector, $\mathbf{A}_i(t) = \mathbf{A}_i(t+T)$, $i = 1, 2$, are $n \times n$ periodic matrices with principal period T, and $\phi(t)$ is an $n \times 1$ initial vector function in the interval $[t_0 - \tau, t_0]$.

We first consider the case where the parametric and delay periods are equal such that $T = \tau$. If $\mathbf{\Phi}(t)$ is the fundamental solution matrix to the non-delay part of Eq. (8), and $\Psi(t)$ is the fundamental solution matrix for the adjoint system such that $\mathbf{\Phi}^{-1}(t) = \Psi(t)^{\mathrm{T}}$, the infinite-dimensional monodromy operator for a periodic DDE system can be defined as [17]

$$(U\mathbf{x})(t) = \mathbf{\Phi}(t)\left\{\mathbf{x}(T) + \int_0^t \Psi(s)^{\mathrm{T}}\mathbf{A}_2(s)\mathbf{x}(s)\,\mathrm{d}s\right\}, \tag{9}$$

which maps continuous functions from the interval $[0, \mathrm{T}]$ back to the same interval, i.e., $U: C[0, T] \to C[0, T]$. We will study the stability of U, that is, the eigenvalues of U. Therefore, it is essential that U act from a vector space of functions back to the same vector space of functions. On the other hand, U is the solution operator of the DDE, Eq. (8), in the sense that if $\mathbf{x}_i(t)$ is a solution on the interval $t \in [i-1, i]$, then $\mathbf{x}_{i+1}(t) = (U\tilde{\mathbf{x}}_i)(t-i)$ is the solution on the interval $t \in [i, i+1]$, where $\tilde{\mathbf{x}}_i(s) = \mathbf{x}_i(s-i+1)$ for $s \in [0, 1]$. Note that Eq. (9) reduces to a well-known formula of the solution to an ODE system once $\mathbf{A}_2(t) \equiv \mathbf{0}$, in which case, U becomes a Floquet transition matrix $\mathbf{\Phi}(T)$. This justifies the name for *U—the delay Floquet transition matrix (DFTM)*. If we directly integrate Eq. (8) from t_0 to t, we obtain

$$\mathbf{x}(t) = \mathbf{x}(t_0) + \int_{t_0}^t (\mathbf{A}_1(s)\mathbf{x}(s) + \mathbf{A}_2(s)\mathbf{x}(s-\tau))\,\mathrm{d}s, \tag{10}$$

where t_0 is an arbitrary initial time. Normalizing the delay period to $\tau = 1$ and setting the initial time to $t_0 = 0$, we obtain the solution vector $\mathbf{x}_1(t)$ in the first interval $[0, 1]$ as

$$\mathbf{x}_1(t) = \mathbf{x}_1(0) + \int_0^t (\mathbf{A}_1(s)\mathbf{x}(s) + \mathbf{A}_2(s)\phi(s-1))\,\mathrm{d}s. \tag{11}$$

Next, we expand $\mathbf{x}_1(t), \mathbf{A}_1(t)$ and $\mathbf{A}_2(t)$ and the initial function $\phi(t-1)$ in m shifted Chebyshev polynomials of the first kind as

$$\mathbf{x}_1(t) = \hat{\mathbf{T}}^{\mathrm{T}}(t)\mathbf{m}_1, \quad \mathbf{A}_1(t) = \hat{\mathbf{T}}^{\mathrm{T}}(t)\mathbf{F},$$

$$\mathbf{A}_2(t) = \hat{\mathbf{T}}^{\mathrm{T}}(t)\mathbf{D}, \quad \phi(t-1) = \hat{\mathbf{T}}^{\mathrm{T}}(t)\mathbf{m}_0,$$

$$\mathbf{x}(0) = \hat{\mathbf{T}}^{\mathrm{T}}(t)\bar{\mathbf{T}}(1)\mathbf{m}_0, \quad 0 \leqslant t \leqslant 1, \tag{12}$$

where $\hat{\mathbf{T}}(t) = \mathbf{I}_n \otimes \mathbf{T}(t), \mathbf{I}_n$ denotes the $n \times n$ identity matrix, $\mathbf{T}(t) = \{T_0^*(t)T_1^*(t)\ldots T_{m-1}^*(t)\}^{\mathrm{T}}$ is an $m \times l$ column vector of the shifted Chebyshev polynomials and $\otimes$ denotes the Kronecker product operation; $\mathbf{m}_1$ and $\mathbf{m}_0$ are the $nm \times 1$ Chebyshev coefficient vectors of the solution vector $\mathbf{x}_1(t)$ and the initial function $\phi(t-1)$, and $\mathbf{F}$ and $\mathbf{D}$ are the $nm \times n$ Chebyshev coefficients matrices of $\mathbf{A}_1(t)$ and $\mathbf{A}_2(t)$ in the first interval $[0, 1]$, respectively. The $nm \times nm$ matrix $\bar{\mathbf{T}}(1)$ is defined as

$$\bar{\mathbf{T}}(1) = \hat{\mathbf{I}}\hat{\mathbf{T}}^{\mathrm{T}}(1) = \mathbf{I}_n \otimes \begin{bmatrix} 1 & \ldots & \ldots & 1 \\ 0 & \ldots & \ldots & 0 \\ \vdots & \vdots & \vdots & \vdots \\ 0 & \ldots & \ldots & 0 \end{bmatrix}_{m\times m}, \tag{13}$$

where $\mathbf{I} = \hat{\mathbf{T}}^{\mathrm{T}}(t)\hat{\mathbf{I}}$. Using the Chebyshev expansions in Eq. (12), Eq. (11) takes the form

$$\hat{\mathbf{T}}^{\mathrm{T}}(t)\mathbf{m}_1 = \hat{\mathbf{T}}^{\mathrm{T}}(t)\bar{\mathbf{T}}(1)\mathbf{m}_0 + \int_0^t (\hat{\mathbf{T}}^{\mathrm{T}}(s)\mathbf{F}\hat{\mathbf{T}}^{\mathrm{T}}(s)\mathbf{m}_1 + \hat{\mathbf{T}}^{\mathrm{T}}(s)\mathbf{D}\hat{\mathbf{T}}^{\mathrm{T}}(s)\mathbf{m}_0)\,\mathrm{d}s. \tag{14}$$

Applying the *integration* and *product* operational matrices $\hat{\mathbf{G}}$ and $\hat{\mathbf{Q}}$ defined in Ref. [13], we obtain

$$\hat{\mathbf{T}}^{\mathrm{T}}(t)\mathbf{m}_1 = \hat{\mathbf{T}}^{\mathrm{T}}(t)\bar{\mathbf{T}}(1)\mathbf{m}_0 + \hat{\mathbf{T}}^{\mathrm{T}}(t)\hat{\mathbf{G}}^{\mathrm{T}}\hat{\mathbf{Q}}_F\mathbf{m}_1 + \hat{\mathbf{T}}^{\mathrm{T}}(t)\hat{\mathbf{G}}^{\mathrm{T}}\hat{\mathbf{Q}}_D\mathbf{m}_0 \tag{15}$$

which can be simplified as

$$[\mathbf{I} - \hat{\mathbf{G}}^{\mathrm{T}}\hat{\mathbf{Q}}_F]\mathbf{m}_1 = [\bar{\mathbf{T}}(1) + \hat{\mathbf{G}}^{\mathrm{T}}\hat{\mathbf{Q}}_D]\mathbf{m}_0. \tag{16}$$

For the ith interval $[i-1, i]$, the linear map $\mathbf{W}$ which relates the Cheybshev coefficient vector $\mathbf{m}_i$ to that in the previous interval is given by inverting the first matrix above as

$$\mathbf{m}_i = [\mathbf{I} - \hat{\mathbf{G}}^{\mathrm{T}}\hat{\mathbf{Q}}_F]^{-1}[\bar{\mathbf{T}}(1) + \hat{\mathbf{G}}^{\mathrm{T}}\hat{\mathbf{Q}}_D]\mathbf{m}_{i-1}. \tag{17}$$

Eq. (17) defines an truncated version of the infinite-dimensional Floquet transition matrix which is given by

$$\mathbf{W} = [\mathbf{I} - \hat{\mathbf{G}}^{\mathrm{T}}\hat{\mathbf{Q}}_F]^{-1}[\bar{\mathbf{T}}(1) + \hat{\mathbf{G}}^{\mathrm{T}}\hat{\mathbf{Q}}_D]. \tag{18}$$

The stability of Eq. (8) is defined by the eigenvalues of $\mathbf{W}$ since it advances the solution forward one period. For asymptotic stability, all the eigenvalues of $\mathbf{W}$ must lie within the unit circle. For neutral stability, it is sufficient that only one (or a pair of complex) eigenvalue(s) lie(s) on the unit circle. If the multiplicity of a critical eigenvalue on the unit circle is more than one, then the system might be unstable.

We next consider the case where the forcing period is an integer multiple of the delay period, i.e., $T = q\tau, q = 2, 3, \ldots$. For simplicity, we start by finding the solution when $T = 2\tau$. The problem under consideration is still Eq. (8). Again, we normalize the time such that $\tau = 1$. Since the matrices $\mathbf{A}_1(t)$ and $\mathbf{A}_2(t)$ must be re-expanded in the second interval $[1, 2]$, using the relationship defined in Eq. (17), we have

$$\mathbf{m}_2 = [\mathbf{I} - \hat{\mathbf{G}}^{\mathrm{T}}\hat{\mathbf{Q}}_{F_2}]^{-1}[\bar{\mathbf{T}}(1) + \hat{\mathbf{G}}^{\mathrm{T}}\hat{\mathbf{Q}}_{D_2}]\mathbf{m}_1, \tag{19}$$

where $\mathbf{F}_2$ and $\mathbf{D}_2$ are the coefficients of Chebyshev of the expansions of $\mathbf{A}_1(t)$ and $\mathbf{A}_2(t)$ in the second interval $[1, 2]$. Note that if we let

$$\mathbf{W}_2 = [\mathbf{I} - \hat{\mathbf{G}}^{\mathrm{T}}\hat{\mathbf{Q}}_{F_2}]^{-1}[\bar{\mathbf{T}}(1) + \hat{\mathbf{G}}^{\mathrm{T}}\hat{\mathbf{Q}}_{D_2}] \tag{20}$$

and denote the $\mathbf{W}$ matrix in the first interval $[0, 1]$ as $\mathbf{W}_1$, then substituting Eqs. (16) and (20) into Eq. (19), we obtain

$$\mathbf{m}_2 = \mathbf{W}_2\mathbf{m}_1 = \mathbf{W}_2\mathbf{W}_1\mathbf{m}_0 = \mathbf{W}\mathbf{m}_0. \tag{21}$$

The entire stability matrix is therefore

$$\mathbf{W} = \mathbf{W}_2\mathbf{W}_1 = [\mathbf{I} - \hat{\mathbf{G}}^{\mathrm{T}}\hat{\mathbf{Q}}_{F_2}]^{-1}[\bar{\mathbf{T}}(1) + \hat{\mathbf{G}}^{\mathrm{T}}\hat{\mathbf{Q}}_{D_2}][\mathbf{I} - \hat{\mathbf{G}}^{\mathrm{T}}\hat{\mathbf{Q}}_{F_1}]^{-1}[\bar{\mathbf{T}}(1) + \hat{\mathbf{G}}^{\mathrm{T}}\hat{\mathbf{Q}}_{D_1}], \tag{22}$$

where $\mathbf{F}_1$ and $\mathbf{D}_1$ are the coefficients of the Chebyshev expansions of $\mathbf{A}_1(t)$ and $\mathbf{A}_2(t)$ in the first interval $[0,1]$. The stability of Eq. (8) for $T=2\tau$ case will be determined by the eigenvalues of Eq. (22).

The general formula of $\mathbf{W}$ matrix of Eq. (8) for $T=q\tau$ can be derived in the same way as

$$\mathbf{W}=\mathbf{W}_q\mathbf{W}_{q-1}\ldots\mathbf{W}_2\mathbf{W}_1, \tag{23}$$

where

$$\mathbf{W}_i=[\mathbf{I}-\hat{\mathbf{G}}^{\mathrm{T}}\hat{\mathbf{Q}}_{F_i}]^{-1}[\bar{\mathbf{T}}(1)+\hat{\mathbf{G}}^{\mathrm{T}}\hat{\mathbf{Q}}_{D_i}]. \tag{24}$$

4. Stability results

4.1. The simple inverted pendulum

In this section, we present the stability charts for the simple and double inverted pendulums by applying the stability criteria described in Section 3. We start with the simple inverted pendulum case. The simplest case is when both the time-periodic and delay effects vanish (i.e. $P_2=\tau=0$) in which the state-space form of the linearized equation is

$$\begin{pmatrix}\dot{x}_1\\ \dot{x}_2\end{pmatrix}=\begin{bmatrix}0 & 1\\ -\alpha^2(1+(\gamma-1)\hat{P}_1) & -\alpha\bar{c}\end{bmatrix}\begin{pmatrix}x_1\\ x_2\end{pmatrix}. \tag{25}$$

(Note that the time coordinate has not been normalized in this case so that $t=\hat{t}$ and $\hat{\tau}=\alpha$.) Eq. (25) is an ordinary differential equation with constant coefficients. The stability of this system requires that $1+(\gamma-1)\hat{P}_1>0$ and $\bar{c}>0$. Note that if $\gamma=1$ then the size of $\hat{P}_1$ is irrelevant for stability since the follower force does not do work. The stability chart in the $[\hat{P}_1,\gamma]$ plane is shown in Fig. 3. The static instability route at the boundary is unaffected by the amount of damping.

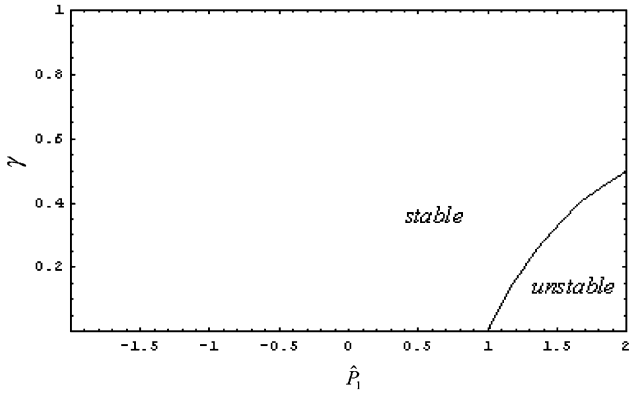

Fig. 3. Stability chart in $\hat{P}_1-\gamma$ plane for the simple inverted pendulum where $\tau=\hat{P}_2=0$.

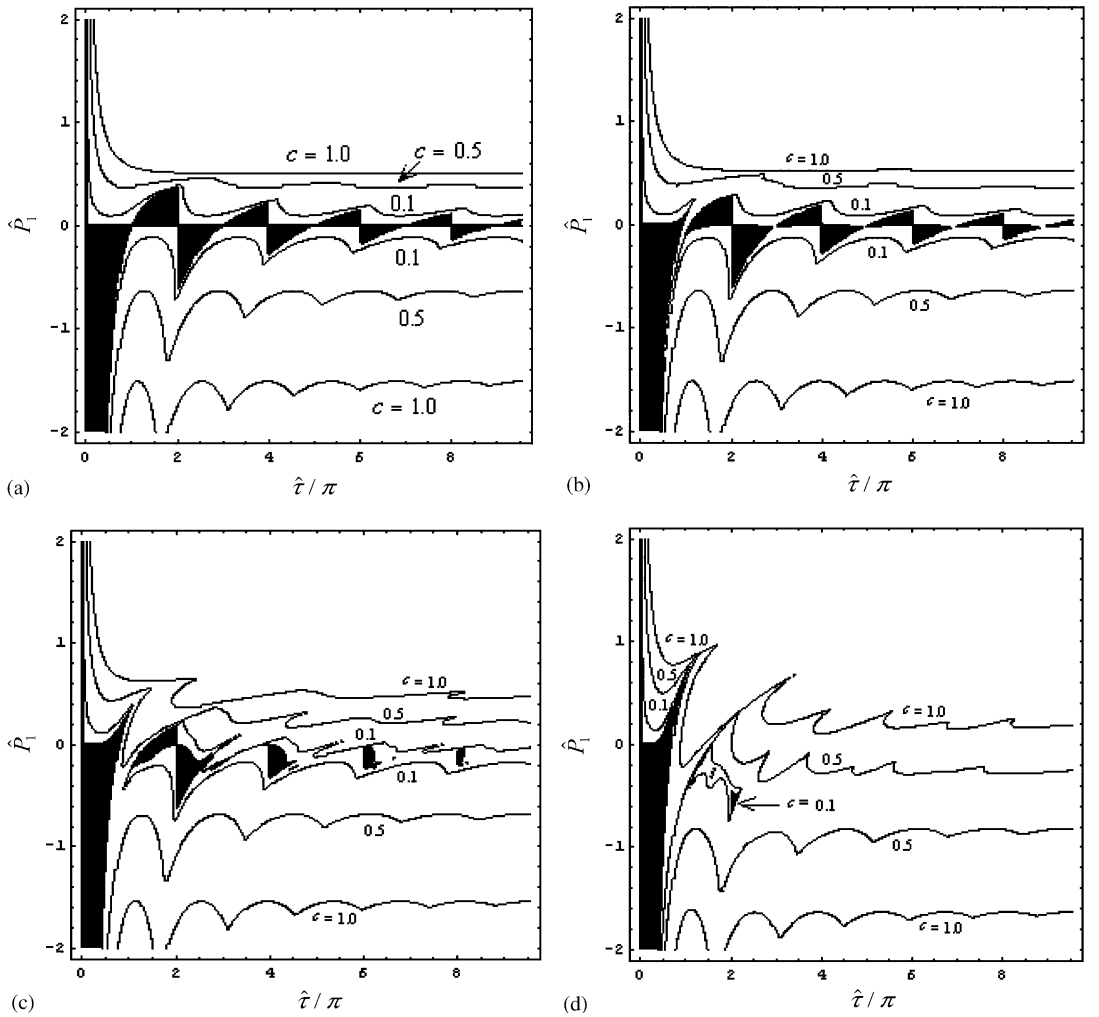

Fig. 4. Stability charts for the simple inverted pendulum where $\gamma = 1$ and $T = \tau$ for various amounts of damping ($c = 0$ in solid black region): (a) $\hat{P}_2 = 0$, (b) $\hat{P}_2 = 0.2$, (c) $\hat{P}_2 = 0.6$, (d) $\hat{P}_2 = 1.2$.

When the time-delay is reinstated and we increase the magnitude of $\hat{P}_2$, these effects are shown in Fig. 4 in the $[\hat{\tau}/\pi, \hat{P}_1]$ plane where $T = \tau$ and $\gamma = 1$ for different values of the damping parameter $\bar{c}$. The method in Section 3 was applied with $m = 55$ Chebyshev polynomials. Note that Fig. 4(a) shows the system with delay but no time-periodic component ($\hat{P}_2 = 0$). This result for the undamped case is the same as the one obtained in Ref. [9]. In Fig. 4(a) it is seen that a small amount of time-delay can cause instability if the damping is small or zero. As we increase the magnitude of the parametric excitation to $\hat{P}_2 = 0.2, 0.6$ and 1.2, the stable region is decreased. In addition, the stability boundaries for the damped ($\bar{c} = 0.1, 0.5, 1.0$) as well as the undamped case are shown in each plot of Fig. 4. In general, it is seen that increasing the damping enlarges the stable region.

The stability effects in Fig. 4 can be explained more precisely by matching the format of Eq. (4) with that of the delayed Mathieu equation

$$\ddot{x} + (\delta + 2\varepsilon\cos 2t)x = (b + 2\varepsilon\cos 2t)x(t - \pi). \tag{26}$$

Note that Eq. (26) is slightly different from the delayed Mathieu equation analyzed in Ref. [18] due to the time-periodic coefficient in the delayed value of x as well as in the non-delayed value. Comparing Eq. (4) with $T = \tau$ and $\gamma = 1$ and the normalized state-space form

$$\begin{pmatrix} \dot{x}_1 \\ \dot{x}_2 \end{pmatrix} = \begin{bmatrix} 0 & 1 \\ -\pi^2(\delta + 2\varepsilon\cos 2\pi\hat{t}) & 0 \end{bmatrix} \begin{pmatrix} x_1 \\ x_2 \end{pmatrix} + \begin{bmatrix} 0 & 0 \\ \pi^2(b + 2\varepsilon\cos 2\pi\hat{t}) & 0 \end{bmatrix} \begin{pmatrix} x_1(\hat{t} - 1) \\ x_2(\hat{t} - 1) \end{pmatrix} \tag{27}$$

of Eq. (26), we find

$$\delta = (\hat{\tau}/\pi)^2(1 - \hat{P}_1), \quad b = -(\hat{\tau}/\pi)^2\hat{P}_1, \quad 2\varepsilon = (\hat{\tau}/\pi)^2\hat{P}_2. \tag{28a–c}$$

The stability charts of Eq. (26) in the $[\delta, b]$ plane for several parameters values of ε are shown in Fig. 5. As shown in Ref. [16], the straight boundaries with slopes of ± 1 for $\varepsilon = 0$ are shifted to the

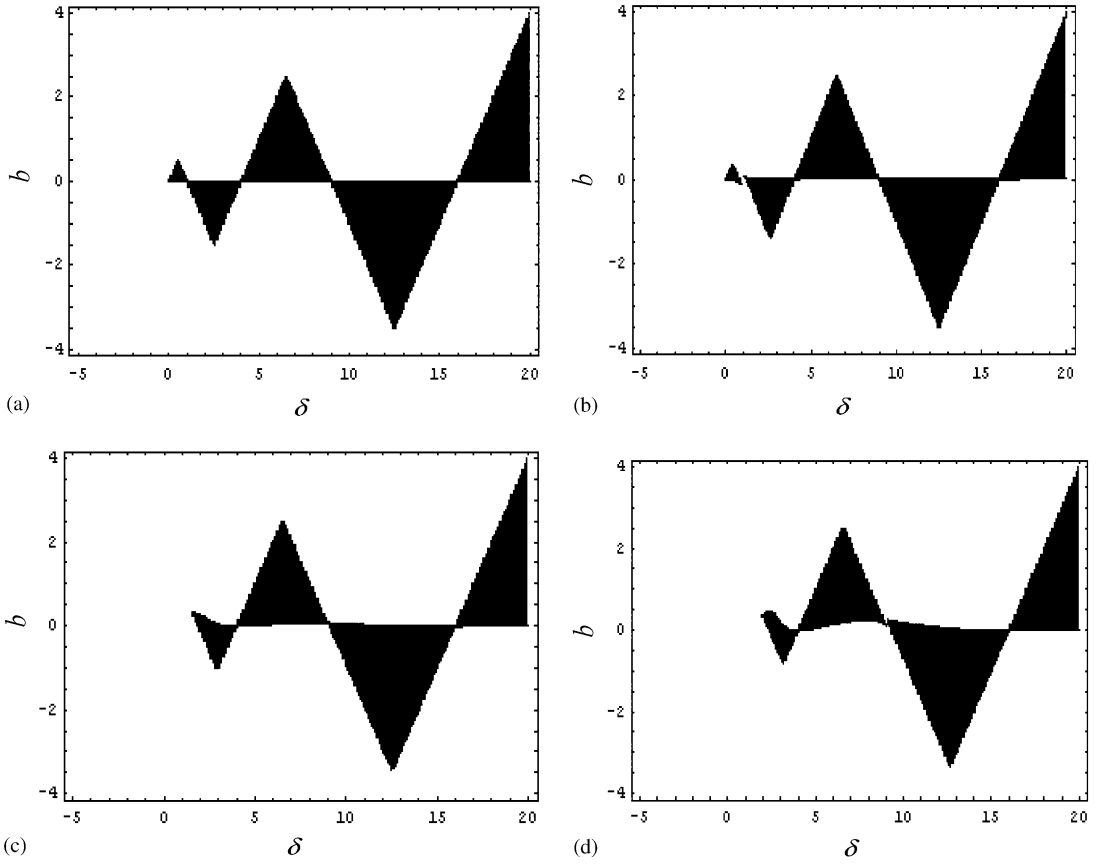

Fig. 5. Stability charts in the $\delta - b$ plane for the delayed Mathieu Eq. (26): (a) $\varepsilon = 0$, (b) $\varepsilon = 0.1$, (c) $\varepsilon = 0.5$, (d) $\varepsilon = 0.9$.

left or right as ε is increased while retaining the same slope. The intercepts of these boundaries with the $(b=0)$ boundary in Fig. 5(a) (which becomes more curved as ε increases) are related to the location of the stability boundaries in the non-delayed Mathieu equation. The analytical form of the boundaries in Fig. 5 can therefore be used to understand and verify the numerical plots in Fig. 4. For example, Fig. 4(a) with $\hat{P}_2=0$ corresponds to $\varepsilon=0$ in Fig. 5(a). Each of the stability boundaries of slope $+1$ in Fig. 5(a) is due to saddle–node bifurcation and corresponds to a vertical stability boundary in Fig. 4(a), while each of the stability boundaries of slope -1 in Fig. 5(a) (also due to saddle–node bifurcation) corresponds to a curved (parabolic) stability boundary in Fig. 4(a). As described in Ref. [9], these boundaries in Fig. 5(a) are given as $\delta=(-1)^n b+n^2$, $n=0,1,2,\ldots$. Using Eq. (28), the corresponding boundaries in Fig. 4(a) are therefore derived as

$$\begin{aligned}&\hat{\tau}/\pi=n, \quad n \text{ even},\\ &(\hat{\tau}/\pi)^2(1-2\hat{P}_1)=n^2, \quad n \text{ odd}.\end{aligned} \tag{29}$$

Finally, the $b=0$ boundary in Fig. 5(a) which destabilizes due to Hopf bifurcation translates to $\hat{P}_1=0$ in Fig. 4(a). As ε is increased in Figs. 5(b–d), the $+1$ slope boundaries have a $+1$ eigenvalue of the $\mathbf{W}$ matrix (indicating fold bifurcation) and the -1 slope boundaries have a -1 eigenvalue of the $\mathbf{W}$ matrix (indicating flip bifurcation). The bifurcation properties of the corresponding boundaries in Figs. 4(b–d) are still preserved.

In Fig. 4(b) when $\hat{P}_2=0.2$, we find each of the curved boundaries in Fig. 4(a) is broken at the point when $\hat{\tau}=i\pi$, $i=1,3,\ldots$. The equations of the first two curved boundaries that intersect $\hat{P}_1=0$ near $\hat{\tau}=\pi$ can be found for $\varepsilon=0.1$ from Eq. (28c), which corresponds to the stability chart for the delayed Mathieu equation in Fig. 5(b). Since the boundary $\delta=-b+1$ in Fig. 5(a) has split into two lines which have slope -1 with $b=0$ intercepts of $\delta_{1b}=0.795125$ and $\delta_{2b}=1.194874$, the equations of these two lines in Fig. 5(b) are

$$\delta=-b+\delta_{1b}=-b+0.795125, \quad \delta=-b+\delta_{2b}=-b+1.194874. \tag{30a,b}$$

Substituting Eqs. (28a) and (28b) into Eqs. (30a) and (30b), we obtain the equations of the first two parabolic boundaries in Fig. 4(b) as

$$\left(\frac{\hat{\tau}}{\pi}\right)^2(1-2\hat{P}_1)=\delta_{1b,2b}. \tag{31}$$

For purpose of comparison, we plot these analytical boundaries (Eq. (31)) along with the numerical boundaries in a small region around $\hat{\tau}=\pi$ in Fig. 6(a) in which it can be seen that the results approximately match each other when $|\hat{\tau}-\pi|$ is small. As is expected, the two boundaries diverge as this quantity becomes large.

As ε is increased the change of the stable region in the (b,δ) plane can be seen in Fig. 5(c) and (d). Fig. 5(d) with $\varepsilon=0.9$ can similarly be used to obtain the two parabolic boundary equations in Fig. 4(b) near $\hat{\tau}=3\pi$. Since the boundary $\delta=-b+9$ in Fig. 5(a) has split into two lines with slope -1 and intercepts of $\delta_{1b}=9.118760$ and $\delta_{2b}=9.28905$ with the broken lines, substituting these values into Eq. (31), we obtain the equations of second two parabolic lines in Fig. 4(b). In Fig. 6(b), we plot the analytical boundaries together with the numerical ones in a small region around $\hat{\tau}=3\pi$. The analytical boundaries are accurate for a wider range of this parameter in this case.

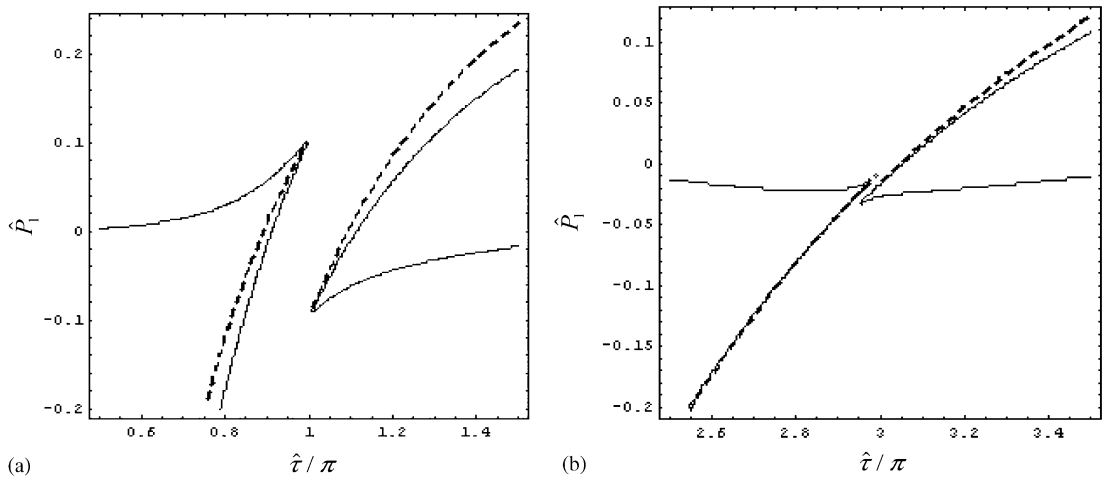

Fig. 6. Comparison of the analytical boundaries (Eq. (31)—dashed) with the numerical boundaries (solid) for $\gamma = 1, c = 0, \hat{P}_2 = 0.2$ near (a) $\hat{\tau} = \pi$, (b) $\hat{\tau} = 3\pi$.

The stability charts for two special values of $\hat{\tau}(\hat{\tau} = \pi, \hat{\tau} = 3\pi)$ in the $[\hat{P}_1, \hat{P}_2]$ plane with $\gamma = 0$ (which surpresses the time-delay term in Eq. (4)) and $\gamma = 1$ are shown in Fig. 7 where $m = 55$. Figs. 7(a) and (c) correspond to the $\gamma = 0$ case when $\hat{\tau} = \pi$ and $\hat{\tau} = 3\pi$, respectively. These plots are similar to those for the non-delayed Mathieu equation (i.e. Eq. (26) with the right-hand side equal to zero) in the (δ, ε) plane. The fact that the plots are reversed with respect to $\hat{P}_1$ follows from Eq. (28a). The boundary intersecting $\hat{P}_2 = 0$ at $\hat{P}_1 = 1$ is the same fold (saddle–node) bifurcation boundary that was seen in Fig. 3, while the parametric resonance-induced unstable regions to the left are due to an alternating sequence of fold and flip bifurcations for which one of the Floquet multipliers is $+1$ and -1, respectively. Figs. 7(b) and (d) correspond to $\gamma = 1$ with $\hat{\tau} = \pi$ and $\hat{\tau} = 3\pi$, respectively. The stable region is largely decreased compared with $\gamma = 0$ case in (a) and (b) due to the time-delay. In addition, the damping effects with $(\bar{c} = 0.1, 0.5, 1.0)$ are also shown. If $\hat{P}_2$ is fixed to one of the four values in Fig. 4 and $\hat{P}_1$ is varied in Figs. 7(b) or (d), the same stability boundaries are intersected as in Fig. 4 if $\hat{\tau}/\pi$ equals 1 or 3, respectively. Hence, these figures can be used to better understand the charts in Fig. 4 near $\hat{\tau} = \pi$ and 3π.

The stability charts for the $T = 2\tau$ case in the $[\hat{\tau}/\pi, \hat{P}_1]$ plane with $\gamma = 1$ for two values of $\hat{P}_2$ are shown in Fig. 8 where $m = 55$ Chebyshev polynomials were used. Here, the stable region corresponds to a spectral radius of matrix $\mathbf{W}$ in Eq. (22) less than unity. Compared to the $T = \tau$ case of Fig. 4(b,c), the $T = 2\tau$ case shows similar stability behaviors. Again, the damping effects are included in each figure.

4.2. The double inverted pendulum

The double inverted pendulum is more complicated than the simple inverted pendulum as the dof of the system becomes 2 involving 4 simultaneous DDEs after being changed into state-space form in Eq. (7). However, we shall see that there are still similar stability effects with those obtained in simple inverted pendulum case.

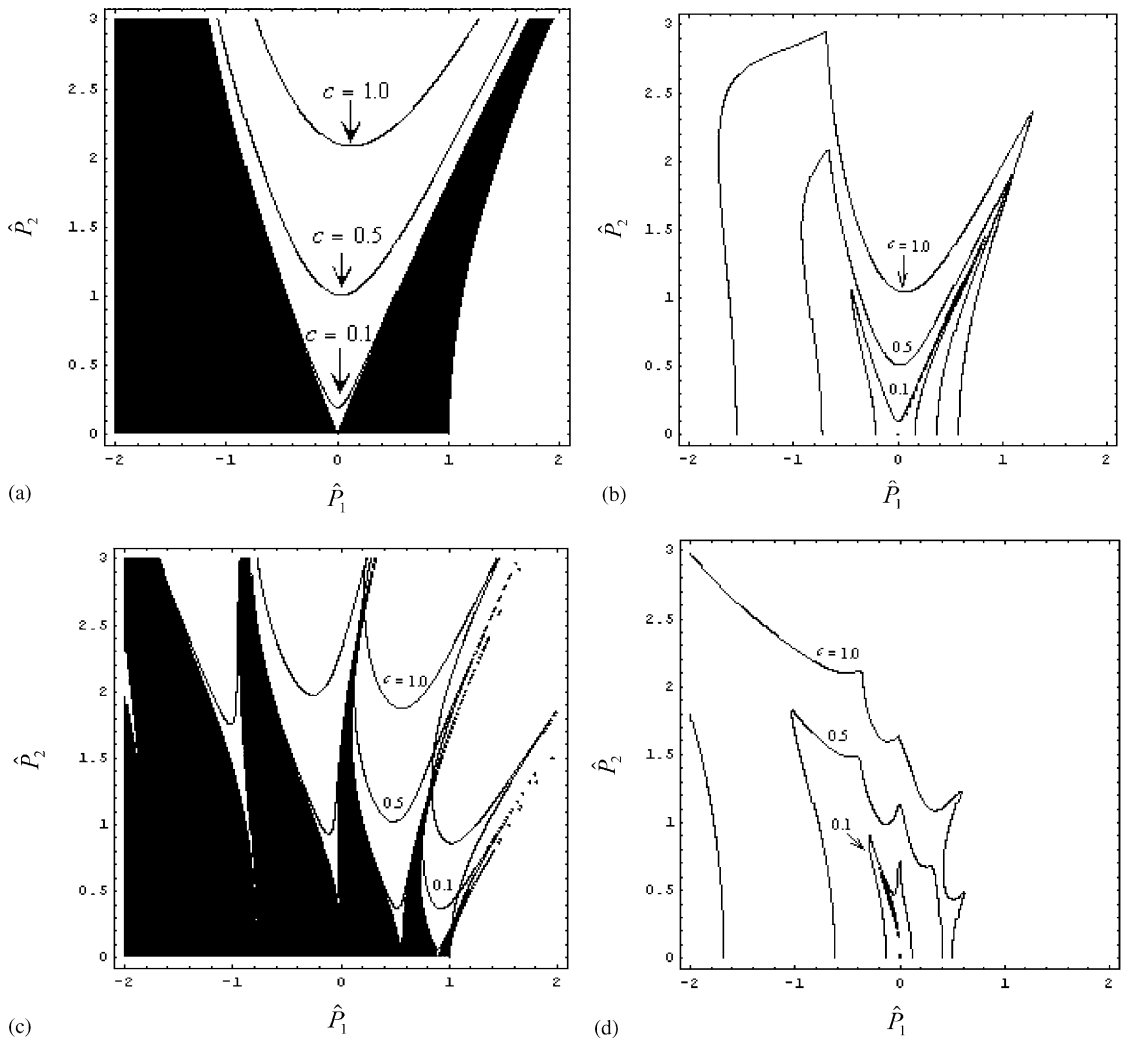

Fig. 7. Stability charts for the simple inverted pendulum for various amounts of damping ($c = 0$ in solid black region): (a) $\gamma = 0, \hat{\tau} = \pi$, (b) $\gamma = 1, \hat{\tau} = \pi$; (c) $\gamma = 0, \hat{\tau} = 3\pi$, (d) $\gamma = 1, \hat{\tau} = 3\pi$.

We begin with the simplest case when $\hat{P}_2$ and τ in Eq. (7) vanish, which yields a set of time-invariant ODEs whose stability properties have been previously analyzed in detail [2–5,12]. The traditional plot in the $(\hat{P}_1, \gamma)$ plane when $\bar{c} = \bar{c}_1 = \bar{c}_2 = 0$ as well as for 3 other values of $\bar{c}$ are reproduced in Fig. 9. The middle curved line which depends on the amount of damping is unstable due to Hopf bifurcation which represents dynamic failure due to flutter [3,12]. The other curved lines represent static failure mode due to divergence (saddle–node bifurcation). As is well-known for nonconservative systems, it is seen here that increasing the damping does not always increase the stable region [5].

Corresponding to Fig. 4 for the simple inverted pendulum we produce stability charts of the double inverted pendulum with time-delay for several values of $\hat{P}_2$ in the $[\hat{\tau}/\pi, \hat{P}_1]$ plane in Fig. 10

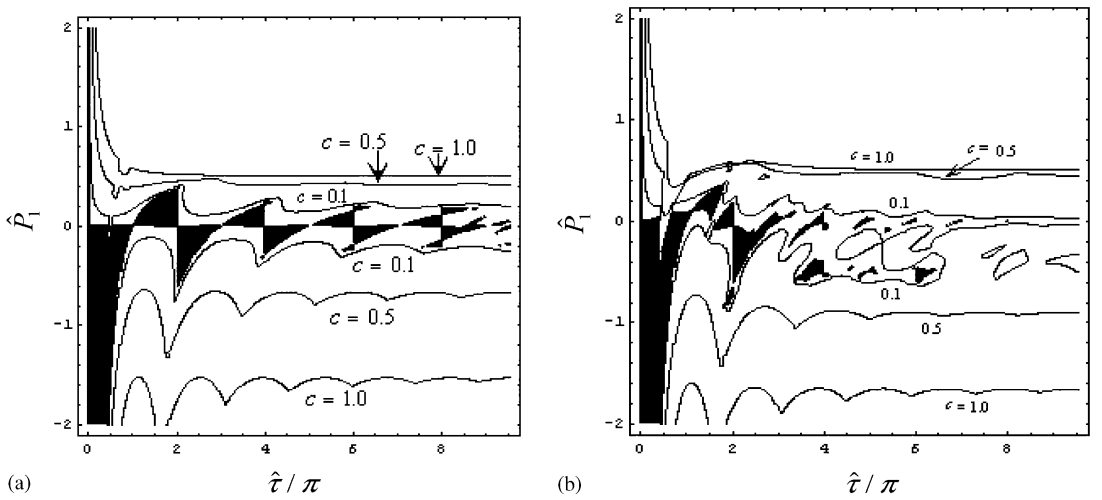

Fig. 8. Stability charts for the simple inverted pendulum where $T = 2\tau, \gamma = 1$ for various amounts of damping ($c = 0$ in solid black region): (a) $\hat{P}_2 = 0.2$, (b) $\hat{P}_2 = 0.6$.

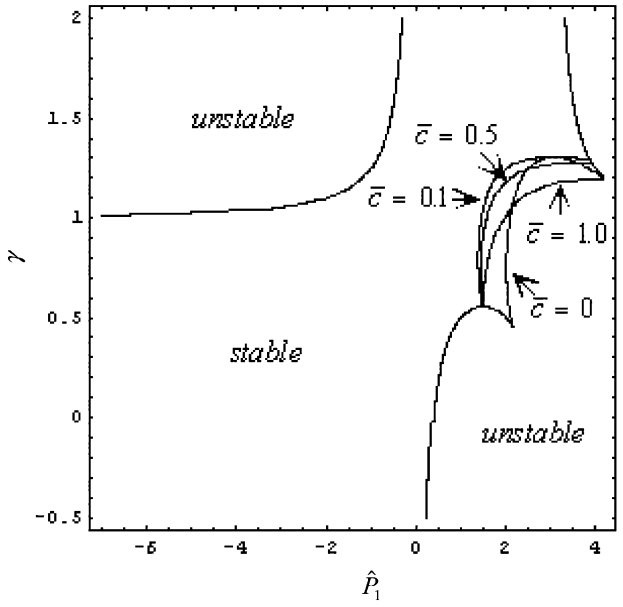

Fig. 9. Stability chart in the $\hat{P}_1 - \gamma$ plane for the double inverted pendulum where $\hat{P}_2 = \tau = 0$ for various amounts of damping.

when $T = \tau, \gamma = 1$, and $m = 55$ Chebyshev polynomials were used. Note that Fig. 10(a) (without parametric excitation) shows the same results that were previously obtained in Refs. [8–10]. As we increase $\hat{P}_2$ from 0 to 0.2, the stable region is seen to decrease. In addition, the boundary lines of the vertical bars below $\hat{P}_1 = 0$ in Fig. 10(b–d) have alternating bifurcation properties. The left-hand side boundaries corresponds to when the spectral radius of the **W** matrix is +1 while the

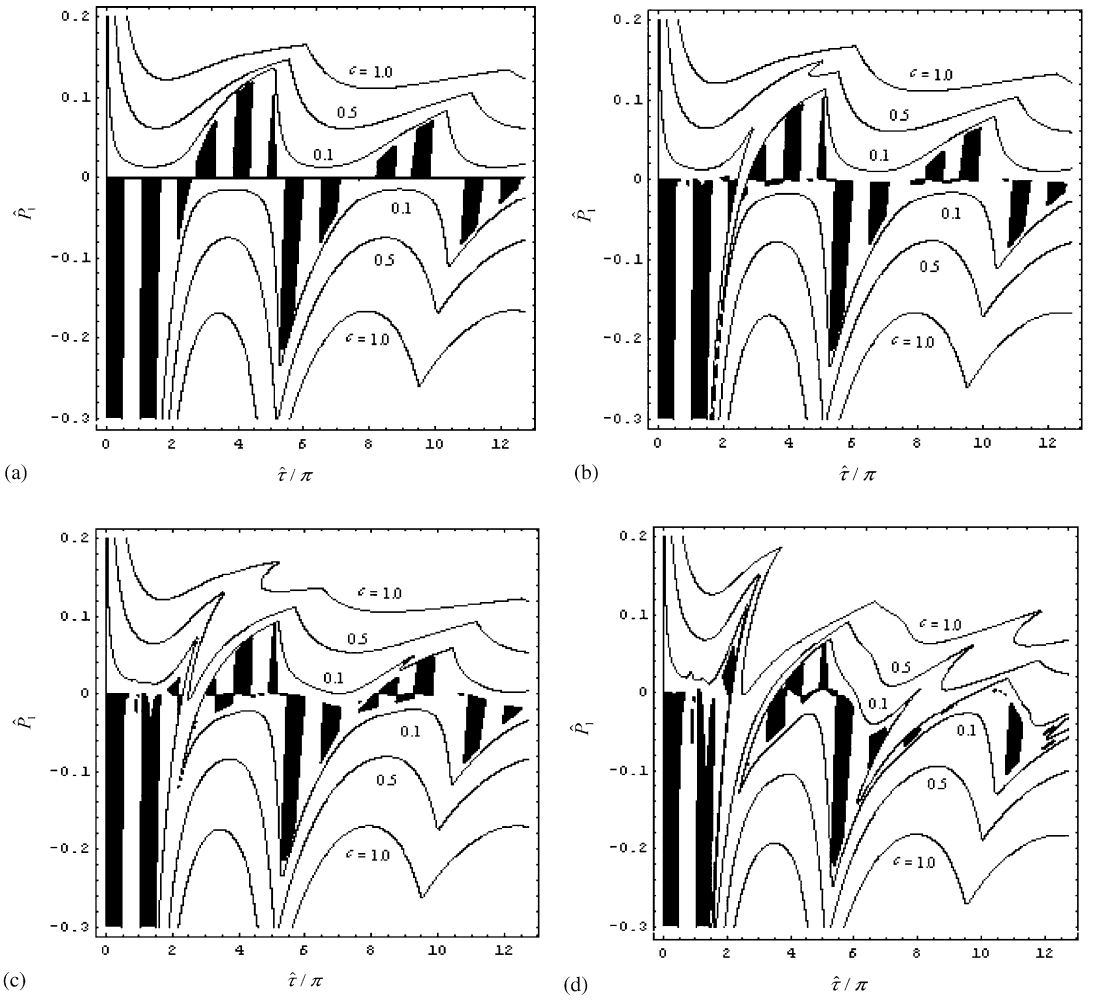

Fig. 10. Stability charts for the double inverted pendulum where $\gamma = 1$ and $T = \tau$ for various amounts of damping ($c = 0$ in solid black region): (a) $\hat{P}_2 = 0$, (b) $\hat{P}_2 = 0.05$, (c) $\hat{P}_2 = 0.1$, (d) $\hat{P}_2 = 0.2$.

ones on the right-hand side have a spectral radius of -1. These show fold and flip bifurcation instability properties, respectively, in the presence of the parametric excitation. In addition, on either side of the $\hat{P}_1 = 0$ line, the curved line on the top of and bottom of each column corresponds to flip bifurcation. Again, in each plot of Fig. 10, the damping effects for $\bar{c} = 0.1, 0.5, 1.0$ are included.

Fig. 11 shows the effect of varying the angle of load γ when $\hat{\tau} = \pi$ for the double inverted pendulum in the $[\hat{P}_1, \hat{P}_2]$ plane where $m = 55$. The stability region in Fig. 11(a) for which the equations of motion are a set of time-periodic ODEs, was first obtained both numerically and symbolically in Ref. [12]. Comparing with the stability charts in Fig. 7, we see that with increasing γ the similar effects of a decreasing stable region occur again. This further shows that introducing the time-delay causes instability. Again, the damping effects are taken into consideration in these plots.

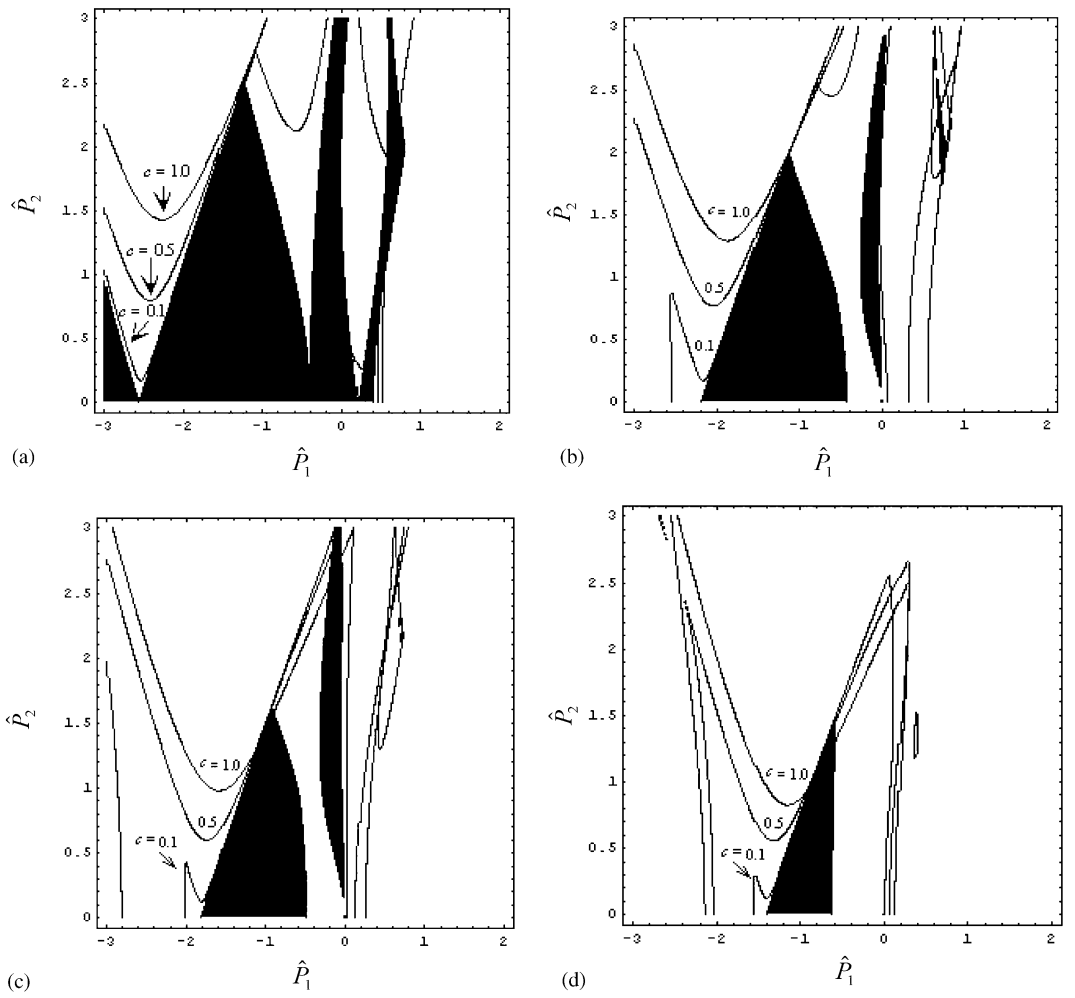

Fig. 11. Stability charts for the double inverted pendulum where $\hat{\tau} = \pi$ for various amounts of damping ($c = 0$ in solid black region): (a) $\gamma = 0$, (b) $\gamma = 0.2$, (c) $\gamma = 0.5$, (d) $\gamma = 1$.

Finally, when $T = 2\tau$, the stability charts for the double inverted pendulum in the $[\hat{\tau}/\pi, \hat{P}_1]$ plane for two values of $\hat{P}_2 (\hat{P}_2 = 0.05, \hat{P}_2 = 0.1)$ with $\gamma = 1$ are shown in Fig. 12. Again, $m = 55$ polynomials were used. They show similar stability behaviors with the ones obtained in Fig. 8 when $T = \tau$ under various damping effects.

5. Conclusion

Stability charts of discretized elastic columns with follower forces which are subjected to both parametric excitation and time-delay effects are first presented by using a shifted Chebyshev-based method. This is possible because the original dynamic system equation can be reduced into a set of

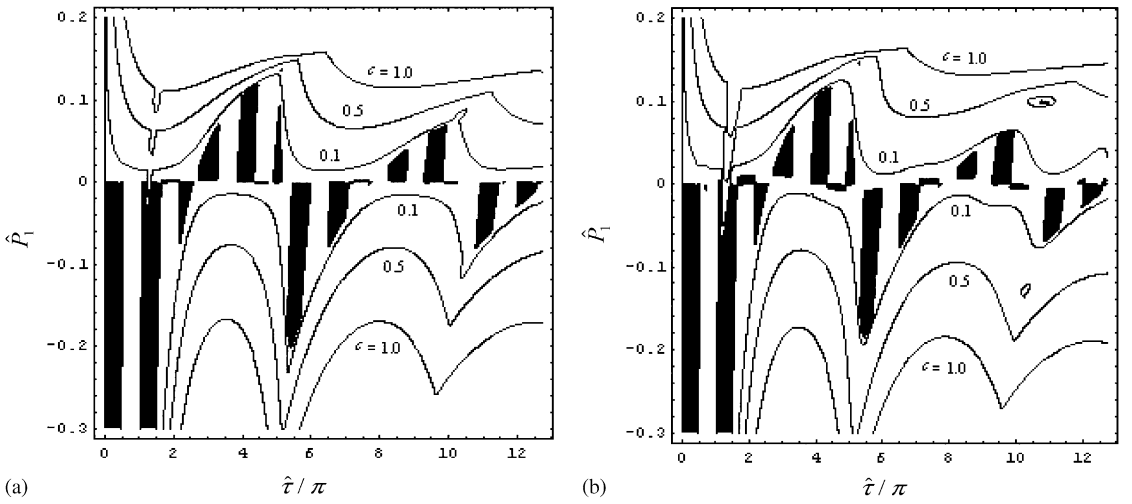

Fig. 12. Stability charts for the double inverted pendulum where $T = 2\tau; \gamma = 1$ for various amounts of damping ($c = 0$ in solid black region): (a) $\hat{P}_2 = 0.05$, (b) $\hat{P}_2 = 0.1$.

difference equations from which the truncated version of "the infinite-dimensional Floquet transition matrix" is found. Therefore, the traditional unit circle stability criteria can be directly applied to this matrix.

A parametrically excited simple pendulum and a double inverted pendulum subjected to a retarded periodic follower force were studied. The results with no delay effects or parametric excitation are exactly the same as the ones reported previously. The results with both parametric excitation and time-delay, which are combined for the first time in this study, show that both effects are generally destabilizing in nature and are thus unwanted. In addition, damping effects and critical values for load direction are taken into consideration. More important, this method explains the fundamental stability phenomena related to delay differential equations (DDEs). It is expected that this method can be applied to solve a wide class of engineering problems which can be modeled as periodic DDEs.

Acknowledgements

This paper is based upon work supported by the National Science Foundation under Grant No. 0114500.

References

[1] M. Beck, Die Knicklast des einseitig eingespannten, tangential gedrückten stabes, *Zeilschrift für angewandle Mathematik and Physik* 3 (1952) 225–228, 476–477.

[2] V.V. Bolotin, *Nonconservative Problems of the Theory of Elastic Stability* (English translation), Macmillan, New York, 1963.
[3] H. Leipholz, *Stability Theory*, Academic Press, New York, 1970.
[4] G. Herrmann, Stability of equilibrium of elastic systems subjected to nonconservative forces, *Applied Mechanics Reviews* 20 (1967) 103.
[5] G. Herrmann, I.-C. Jong, On the destabilizing effect of damping in nonconservative elastic systems, *Journal of Applied Mechanics* 32 (3) (1965) 592–597.
[6] J. Guckenheimer, P. Holmes, *Nonlinear Oscillations, Dynamical Systems, and Bifurcations of Vector Fields*, Springer, New York, 1983.
[7] K. Husseyin, *Vibrations and Stability of Multiple Parameter Systems*, Noordhoff International Publishing, 1978.
[8] C.S. Hsu, Application of the tau-decomposition method to dynamical systems subjected to retarded follower forces, *Journal of Applied Mechanics* 37 (1970) 258–266.
[9] G. Stepan, *Retarded Dynamical Systems*, Longman, Harlow, UK, 1989.
[10] J. Kiusalaas, H.E. Davis, On the stability of elastic systems under retarded follower forces, *International Journal of Solids and Structures* 6 (1970) 399–409.
[11] V.A. Yakubovich, V.M. Starzhinski, *Linear Differential Equations with Periodic Coefficients—Part I*, Wiley, New York, 1975.
[12] E.A. Butcher, S.C. Sinha, Symbolic computation of local stability and bifurcation surfaces for nonlinear time-periodic systems, *Nonlinear Dynamics* 17 (1998) 1–21.
[13] S.C. Sinha, E.A. Butcher, Symbolic computation of fundamental solution matrices for linear time-periodic dynamical systems, *Journal of Sound and Vibration* 206 (1) (1997) 61–85.
[14] E.A. Butcher, H.-T. Ma, E. Bueler, V. Averina, Z. Szabo, Stability of time-periodic delay-differential equations via Chebyshev polynomials, *International Journal of Numerical Methods in Engineering* 59 (2004) 895–922.
[15] T. Insperger, G. Stepan, Semi-discretization method for delayed systems, *International Journal of Numerical Methods in Engineering* 55 (2002) 503–518.
[16] K. Engelborghs, T. Luzyanina, K.J. in't Hout, D. Roose, Collocation methods for the computation of periodic solutions of delay differential equations, *SIAM Journal of Scientific Computation* 22 (2000) 1593–1609.
[17] J. Hale, S.M. Verduyn Lunel, *Introduction to Functional Differential Equations*, Springer, Berlin, 1993.
[18] T. Insperger, G. Stepan, Stability chart for the delayed Mathieu equation, *Proceedings of The Royal Society, Mathematical, Physical and Engineering Sciences* 458 (2024) (2002) 1989–1998.